Molecular Microbiology (2015) 96(1), 4–13 ■
doi:10.1111/mmi.12834
First published online 4 November 2014

Single-molecule tracking in live *Vibrio cholerae* reveals that ToxR recruits the membrane-bound virulence regulator TcpP to the *toxT* promoter

Beth L. Haas,[1] Jyl S. Matson,[2] Victor J. DiRita[3]* and Julie S. Biteen[1]**

[1]*Department of Chemistry, University of Michigan, Ann Arbor, MI 48109, USA.*
[2]*Department of Medical Microbiology and Immunology, University of Toledo Medical School, Toledo, OH 43614, USA.*
[3]*Department of Microbiology and Immunology, University of Michigan Medical School, Ann Arbor, MI 48109, USA.*

Summary

Vibrio cholerae **causes the human disease cholera by producing a potent toxin. The** ***V. cholerae*** **virulence pathway involves an unusual transcription step: the bitopic inner-membrane proteins TcpP and ToxR activate** ***toxT*** **transcription. As ToxT is the primary direct transcription activator in** ***V. cholerae*** **pathogenicity, its regulation by membrane-localized activators is key in the disease process. However, the molecular mechanisms by which membrane-localized activators engage the transcription process have yet to be uncovered in live cells. Here we report the use of super-resolution microscopy, single-molecule tracking, and gene knockouts to examine the dynamics of individual TcpP proteins in live** ***V. cholerae*** **cells with < 40 nm spatial resolution on a 50 ms timescale. Single-molecule trajectory analysis reveals that TcpP diffusion is heterogeneous and can be described by three populations of TcpP motion: one fast, one slow, and one immobile. By comparing TcpP diffusion in wild-type** ***V. cholerae*** **to that in mutant strains lacking either** ***toxR*** **or the** ***toxT*** **promoter, we determine that TcpP mobility is greater in the presence of its interaction partners than in their absence. Our findings support a mechanism in which ToxR recruits TcpP to the** ***toxT*** **promoter for transcription activation.**

Accepted 14 October, 2014. For correspondence. *E-mail vdirita@umich.edu; Tel. (+1) 734 936 3804; Fax (+1) 734 764 3562; **E-mail jsbiteen@umich.edu; Tel. (+1) 734 647 1135; Fax (+1) 734 647 1179.

Introduction

Cholera is a waterborne disease that continues to threaten human populations, as evidenced by the 2010 outbreak in Haiti (Cravioto *et al.*, 2011). The *Vibrio cholerae* bacterium causes disease by colonizing the human gut, where it produces an enterotoxin called cholera toxin (Mekalanos, 2010). Cholera toxin alters enterocyte physiology, leading to the opening of normally gated channels and release of ions and water; this infection manifests itself in the patient as voluminous secretory diarrhea. Although rehydration therapy and antibiotics can treat the symptoms and stop the bacteria from causing further harm to a patient (Matson *et al.*, 2007), cholera remains a threat to human health in many low- and middle-income countries. Understanding the mechanisms by which *V. cholerae* produces its potent toxin will provide avenues for developing novel therapeutic approaches.

The cytoplasmic ToxT protein activates transcription of cholera toxin and other associated virulence factors (Beck *et al.*, 2004), but ToxT expression is regulated by an unusual membrane-associated mechanism: the bitopic proteins TcpP and ToxR cooperate to activate *toxT* transcription while remaining localized to the inner membrane (Fig. 1; Crawford *et al.*, 2003; Matson *et al.*, 2007). TcpP is the direct *toxT* transcription activator, while ToxR plays an accessory role, enhancing DNA binding or transcription activation by TcpP (Häse and Mekalanos, 1998; Krukonis *et al.*, 2000; Matson *et al.*, 2007). Although several models for *toxT* transcription activation have been proposed based on biochemical evidence (Krukonis and DiRita, 2003a; Goss *et al.*, 2010; 2013), the coordination of TcpP and ToxR – and their interactions with other components of the transcription complex – have yet to be observed directly in cells; the mechanistic details of these protein–protein and protein–DNA interactions therefore remain unclear.

TcpP and other proteins are too small (< 5 nm) to see using traditional light microscopy, and the short timescale of protein–protein interactions makes them too dynamic for electron microscopy. Single-molecule fluorescence (SMF) microscopy bridges the gap between the limits of conventional microscopy and the size of macromolecules, and reveals dynamic interactions occurring on size scales

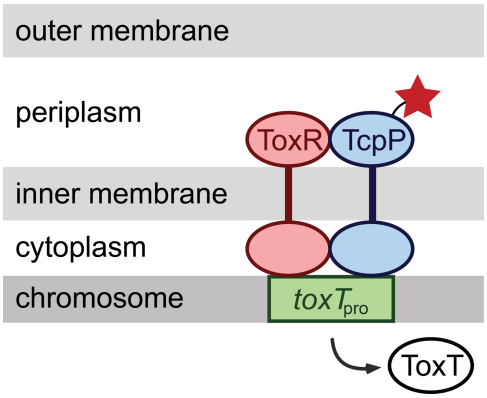

Fig. 1. Schematic of the ToxR regulon. ToxR and TcpP bind the *toxT* promoter ($toxT_{pro}$) and activate ToxT transcription. In this study, TcpP is labeled with the fluorescent protein PAmCherry in the periplasm (star).

below the ~ 300 nm diffraction limit of visible light (Qian *et al.*, 1991; Thompson *et al.*, 2002). Furthermore, the high sensitivity of SMF imaging enables detection of individual fluorescent labels using traditional wide-field microscopy. The center of each emission spot indicates the position of the individual molecule with 10–40 nm resolution, and in living cells, fluorescent protein fusions provide highly specific labels that can be detected, mapped and tracked non-invasively (Griffin *et al.*, 1998). SMF microscopy has been applied to model bacterial systems (Biteen *et al.*, 2008; Xie *et al.*, 2008; Wang *et al.*, 2011; Bakshi *et al.*, 2012), and is now being extended beyond model bacterial systems to investigations of infectious microbes (Berk *et al.*, 2012). Here we apply single-molecule detection and tracking to study a key regulatory event inside a pathogenic bacteria cell.

Based on super-resolution imaging with Photoactivated Localization Microscopy (PALM; Betzig *et al.*, 2006; Hess *et al.*, 2006; Rust *et al.*, 2006) and quantitative analysis of single-molecule trajectories (Qian *et al.*, 1991; Schütz *et al.*, 1997; Lommerse *et al.*, 2004; Kim *et al.*, 2006; Jaqaman *et al.*, 2008), we uncover the molecular-scale interactions and dynamics of TcpP in live *V. cholerae*. In particular, we find that the highly heterogeneous movements of TcpP can be categorized into three populations: one fast, one slow, and one immobile. By using genetic knockouts, we compare TcpP diffusion in wild-type cells to that in cells lacking either *toxR* (Δ*toxR*) or the *toxT* promoter ($toxT_{\Delta pro}$). Overall, we find that TcpP moves faster in the presence of both interaction partners than it does in cells lacking either one of those factors, which implies that (1) binding at the *toxT* promoter mediates interaction between ToxR and TcpP, and (2) the presence of ToxR increases TcpP mobility. Our findings support a mechanism in which ToxR recruits TcpP to the *toxT* promoter for *toxT* transcription activation.

Results

In vitro *characterization confirms TcpP–PAmCherry fusion activity*

We monitored the motion of a TcpP–PAmCherry fusion expressed from an arabinose-inducible promoter in Δ*tcpP V. cholerae*. Immunoblotting with anti-TcpP serum demonstrated that the TcpP–PAmCherry fusion is intact and stable (Fig. S1A). Real-time reverse-transcription PCR (qRT-PCR) determined that Δ*tcpP* TcpP–PAmCherry cells induced under the same conditions used for the microscopy experiments (*Experimental procedures*) activate *toxT* transcription at approximately the same level as wild-type cells (0.8×). The TcpP–PAmCherry protein fusion also complemented the Δ*tcpP* strain for expression of the ToxT-controlled toxin-coregulated pilus protein TcpA (Fig. S1B). Taken together, these results confirm that TcpP–PAmCherry is functional in *V. cholerae*, and that our labeled system is comparable to the wild-type system, which has a fully functional ToxR regulon. We refer to this cell strain as WT* in subsequent discussion (Table 1).

Live-cell single-molecule imaging reveals TcpP positions and trajectories

WT* *V. cholerae* cells grown in virulence-inducing conditions in minimal media with arabinose were imaged using 405 nm light for photo-activation and 561 nm light for excitation. All TcpP–PAmCherry was initially undetectable. After photo-activation, up to three copies of TcpP–PAmCherry were visible in each cell at a time, and the emission from these molecules was recorded until they all photobleached. Through repeated cycles of photo-activation and imaging over 5–7 min, 10–50 TcpP–PAmCherry molecules were detected in each cell. We determined the position of each TcpP molecule in each 50 ms imaging frame with sub-pixel resolution (< 40 nm). PALM super-resolution images of the TcpP positions in the cells were reconstructed from these localizations (Fig. 2A). Furthermore, single-molecule trajectories were created by connecting TcpP–PAmCherry localizations within 6 pixels (294 nm) in consecutive frames (Fig. 2B; Haas *et al.*, 2014). Most single-frame displacements were smaller than

Table 1. Summary of strains used for imaging.

	Strain	Reference
WT*	O395 Δ*tcpP* (RY1)	Yu and DiRita (1999)
Δ*toxR*	O395 Δ*tcpP* Δ*toxR* (EK459)	Krukonis *et al.* (2000)
$toxT_{\Delta pro}$	O395 Δ*tcpP* $toxT_{\Delta pro}$ (EK1647)	Goss *et al.* (2010)

Cells strains and abbreviations used. TcpP–PAmCherry was expressed in all three strains from the plasmid pBAD18-Kan (Guzman *et al.*, 1995).

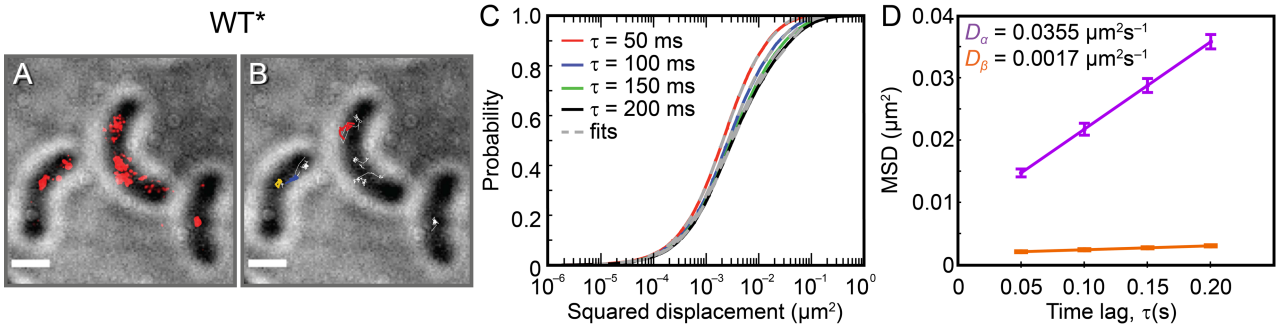

Fig. 2. Localization and dynamical information from single-molecule imaging in WT* cells.
A. Representative PALM super-resolution reconstructions (red) from 20–40 s of image capture overlaid on reverse-contrast bright-field images of WT* *V. cholerae* cells. Only molecules localized with resolutions better than 40 nm are included.
B. Representative single-molecule trajectory maps from the data in A (white) overlaid on the same reverse-contrast bright-field cell image. Only trajectories lasting at least 0.50 s (10 frames) are shown. Three trajectories are highlighted (red, yellow, blue) to show the variety of motion observed. Additional trajectories are plotted in white.
C. Cumulative probability distribution (CPD) of squared displacements for each of the first four time lags (50, 100, 150 and 200 ms in red, blue, green, black respectively) and best fit three-term CPD models (Eq. S3) (2 mobile populations and 1 immobile population; dashed gray lines).
D. Population mean squared displacement (MSD) versus time lag, τ, for the 'fast' and 'slow' populations. The slopes of the two curves are proportional to the fast diffusion coefficient, D_α, and the slow diffusion coefficient, D_β, respectively. Error bars: ±1 standard deviation.
Scale bars: 1 μm.

100 nm (Table 2). Only trajectories lasting at least 0.50 s (localizations in 10 consecutive imaging frames) were included in further analysis. The PALM images and tracks of three representative cells in Fig. 2A and B, respectively, indicate that TcpP is dynamic and explores the entire *V. cholerae* membrane.

Single-molecule trajectory analysis measures TcpP dynamics

Figure 2A and B qualitatively depicts TcpP motion in *V. cholerae*. However, understanding TcpP dynamics in the context of protein–protein and protein–DNA interactions requires a more quantitative trajectory analysis. Determining the mean squared displacement (MSD) of single-molecule tracks provides the diffusion coefficient, D, for each individual molecule observed (Eq. S1; Fig. S2). However, because D is directly proportional to MSD only in the case of homogeneous Brownian motion, this D is only an average value which obscures the details of a heterogeneous molecular trajectory. For instance, in the present study, if TcpP scans DNA freely at first and then becomes immobile when it binds to the *toxT* promoter, a single-molecule MSD curve would not separate the two behaviors and would instead reflect some average behavior (Michalet, 2011). Therefore, to overcome this limitation of MSD analysis and to quantify heterogeneous TcpP dynamics, we consider the cumulative probability distribution (CPD; Eq. S2) of all TcpP displacements (Schütz *et al.*, 1997; Sonnleitner *et al.*, 1999; van den Wildenberg *et al.*, 2011). Here, we fit distributions of squared displacements at each time lag, τ, to a model distribution (Eq. S3) that explicitly allows for heterogeneity in order to categorize the collective motion of all TcpP molecules into multiple populations, each with a distinct diffusion coefficient and a measured contribution to the whole.

Table 2. Number of cells and trajectories studied.

Strain	Cells	Trajectories	Displacements	Mean displacement (nm)
WT*	74	1083	21057	59.3
Δ*toxR*	119	1144	22358	55.4
$toxT_{\Delta pro}$	54	2609	45225	56.8

Only trajectories lasting at least 0.50 s (10 consecutive imaging frames) were included. Displacements between two consecutive 50 ms imaging frames were used for the histograms in Fig. 4. The standard error of the mean for all three strains is < 0.35 nm.

The CPDs of squared TcpP displacements for time lags of τ = 50, 100, 150 and 200 ms are plotted in Fig. 2C in red, blue, green and black respectively. These data are well described (fit shown with dashed grey curves) by a model with three different populations of TcpP motion (Eq. S3): a 'fast' population, a 'slow' population, and a population that is immobile within our < 40 nm resolution. A model with three free mobile terms also identified this immobile term and yielded essentially the same diffusion coefficient results, and models with fewer terms fit poorly (Fig. S3). According to Eq. S3, the two mobile populations are each described by an MSD value at each time lag. Diffusion coefficients for each mobile population can be determined from the slopes of their respective MSD curves (Fig. 2D; Eq. S1). The CPD and MSD curves in Fig. 2C

Table 3. Summary of cumulative probability distribution results.

Strain	α (%)	β (%)	γ (%)	D_α ($\times 10^{-3}$ μm^2 s^{-1})	D_β ($\times 10^{-3}$ μm^2 s^{-1})
WT*	29.4 ± 0.6	48.4 ± 0.5	22.2 ± 0.8	35.5 ± 2.0	1.7 ± 0.3
Δ*toxR*	21.3 ± 0.7	53.7 ± 0.6	25.0 ± 0.9	23.4 ± 3.2	0.8 ± 0.3
$toxT_{\Delta pro}$	26.8 ± 0.6	59.1 ± 0.4	14.1 ± 0.7	18.8 ± 1.3	1.0 ± 0.3

Fractional contributions for the 'fast', 'slow', and immobile terms (α, β, and γ respectively), as well as the diffusion coefficients for the mobile terms (D_α and D_β). Errors are ± 1 standard deviation, and the differences between values for each strain are significant ($P < 0.001$) for pairwise *t*-test comparisons of each variable.

and D reveal that 29.4% of the TcpP motion in WT* forms a 'fast' mobile population with $D_\alpha = 35 \times 10^{-3}$ μm^2 s^{-1}, that almost half (48.4%) of the TcpP motion is in the 'slow' population and more than an order of magnitude slower ($D_\beta = 1.7 \times 10^{-3}$ μm^2 s^{-1}), and that the slowest 22.2% of the TcpP motion is immobile within our < 40 nm resolution. Importantly, the relatively small diffusion coefficients for both the 'fast' and 'slow' populations are too small to be attributed to freely diffusing protein in the periplasm – which would be the case if the fusion protein were subject to significant proteolysis, thereby liberating the PAmCherry domain – for which diffusion coefficients of ~ 2–5 μm^2 s^{-1} are expected (Sochacki *et al.*, 2011). Fractional contributions of each term and diffusion coefficients for the mobile populations are presented in Table 3.

TcpP diffuses faster in the presence of ToxR and the toxT promoter

To investigate the impact of protein–protein and protein–DNA interactions on TcpP diffusion, we compared the TcpP–PAmCherry motion in WT* *V. cholerae* to TcpP–PAmCherry motion in strains lacking either the ToxR interaction partner (Δ*toxR*) or the *toxT* promoter region [$toxT_{\Delta pro}$; position –112 to +1 relative to the start of *toxT* transcription (Krukonis *et al.*, 2000; Goss *et al.*, 2010); Table 1]. The PALM images and tracks from live-cell SMF imaging are shown in Fig. 3A and B for two representative Δ*toxR* cells, and in Fig. 3C and D for two representative $toxT_{\Delta pro}$ cells.

Figure 4A shows the normalized histogram of all frame-to-frame displacements in each of the three cell strains. At our 20 frames per second imaging rate, each measurement indicates the displacement per 50 ms. In all three mutants, Fig. 4A shows a broad distribution of displacement sizes, consistent with the existence of several different types of motion. However, there are notable differences among the three cell types. In particular, TcpP makes more very large displacements (> 100 nm) when both of its interaction partners are present (WT*) and more smaller displacements in their absence (Δ*toxR*, $toxT_{\Delta pro}$; Fig. 4B). This difference is also reflected in the mean displacement length for each strain (Table 2): the mean displacement in WT* (59.3 nm) is greater than the mean displacement in the knockout strains Δ*toxR* (55.4 nm) and $toxT_{\Delta pro}$ (56.8 nm). The numbers of cells, trajectories, and displacements used in these histograms are given in Table 2. The standard error of the mean for all three strains was < 0.35 nm.

In order to make comparisons among the three strains, we examined the CPDs of squared TcpP displacements in Δ*toxR* (Fig. 5A and B) and $toxT_{\Delta pro}$ (Fig. 5C and D). As was found for WT*, the knockout strains were well described by a three-term model (Eq. S3). The diffusion coefficients for the mobile populations differed among the strains, as did the amount each population contributed to the model (Fig. 6A; Table 3). Importantly, the diffusion coefficients for both the 'fast' and 'slow' populations are larger in WT* than in the knockout strains. Additionally, we examined all mobile displacements and compared the fraction of motion described by the 'fast' population to the fraction in

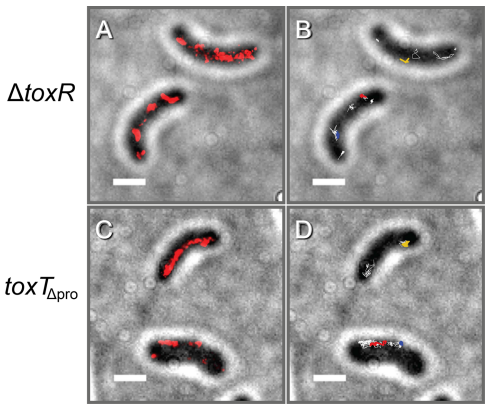

Fig. 3. Representative PALM reconstructions and single-molecule trajectory maps for genetic knockout *V. cholerae* cells.
A and C. Super-resolution reconstructions (red) from 20–40 s of image capture overlaid on reverse-contrast bright-field images of Δ*toxR* and $toxT_{\Delta pro}$ *V. cholerae* cells respectively. Only molecules localized with resolutions better than 40 nm are included.
B and D. Single-molecule trajectories from the data in A and C respectively (white) overlaid on the same reverse-contrast bright-field cell images. Only trajectories lasting at least 0.50 s (10 frames) are shown. Three trajectories are highlighted (red, yellow, blue) to show the variety of motion observed. Additional trajectories are plotted in white.
Scale bars: 1 μm.

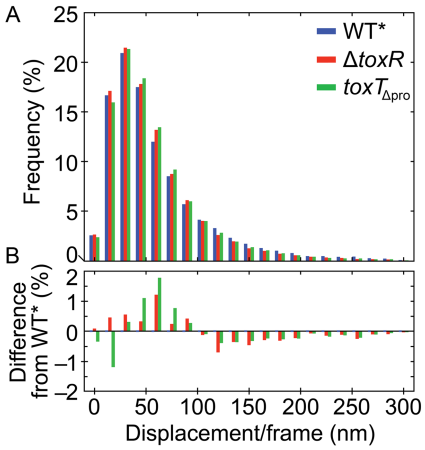

Fig. 4. TcpP displacement lengths.
A. Histogram of sizes of displacements between consecutive 50 ms imaging frames in the three mutants: WT* (blue), Δ*toxR* (red), and $toxT_{\Delta pro}$ (green). The histogram data are aggregated across multiple experiments and normalized by the total number of displacements measured. The number of cells, trajectories, and displacements measured are listed in Table 2.
B. Differences between the histograms of the knockout strains (Δ*toxR*, red, and $toxT_{\Delta pro}$, green) and the WT* strain (blue).

the 'slow' population (Fig. 6B) and found a greater contribution from the 'fast' population in WT* than in either of the knockouts ('fast' fraction = 37.8%, 28.4%, and 31.2% for WT*, Δ*toxR*, and $toxT_{\Delta pro}$ respectively).

An immobile TcpP population exists in all three mutant strains

In all three cell types examined, the best fit CPD (Eq. S3) included a significant immobile population, (Table 3; Fig. 6C). The immobile fraction is smaller, but not fully absent in cells lacking the *toxT* promoter (14.1% in $toxT_{\Delta pro}$ versus 22.2% in WT*), indicating that TcpP binding to $toxT_{pro}$ accounts for some, but not all, of the observed immobile population. We attribute some of this immobile population to imaging artifacts arising from capturing inherently three-dimensional motion (along the curved *V. cholerae* membrane) as a two-dimensional image. Movements perpendicular to the cell length – particularly those at the edges of the projection – appear shorter than movements in the longitudinal direction (Fig. S4A, green and purple curves respectively). Monte Carlo simulations of molecules diffusing randomly on the surface of a cylinder indicate that the actual diffusion coefficient is captured by our CPD analysis. However, for the relevant diffusion rates and dimensions, these simulations also determine that curvature artifacts can account for an apparent immobile population that contributes $\gamma = 2$–6% to the model (Fig. S4B and C). Still, in our experiments, we measure $\gamma > 14\%$ for all strains, indicating that, despite this artifact, a significant immobile TcpP–PAmCherry population remains, even in the absence of $toxT_{\Delta pro}$. This implies that specific DNA-binding at the *toxT* promoter is insufficient to explain the observed immobile population.

Discussion

TcpP binding to the toxT promoter produces a significant increase in observations of immobilized TcpP molecules

Because our 20 frames per second imaging condition is selected to detect only the slowest TcpP molecules ($D < 4 \times 10^{-2}$ μm^2 s^{-1}; Kim *et al.*, 2006), we attribute all of our trajectories to observations of the bitopic inner membrane protein TcpP interacting with the chromosome.

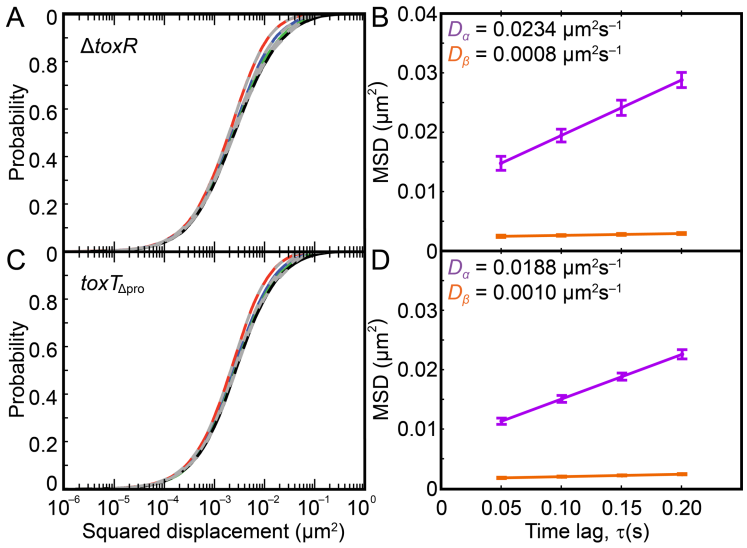

Fig. 5. Cumulative probability distributions (CPDs) and population mean squared displacements (MSDs) for genetic knockout *V. cholerae* strains.
A and C. Cumulative probability distributions of squared displacements for each of the first four time lags (50, 100, 150 and 200 ms in red, blue, green, black respectively) and best fit three-term CPD models (Eq. S3) (2 mobile populations and 1 immobile population; dashed gray lines).
B and D. Population MSD versus time lag, τ, for the 'fast' and 'slow' populations in both of the genetic knockout strains. The slope of each curve is proportional to the fast diffusion coefficient, D_α, or the slow diffusion coefficient, D_β, respectively. Error bars: ±1 standard deviation.

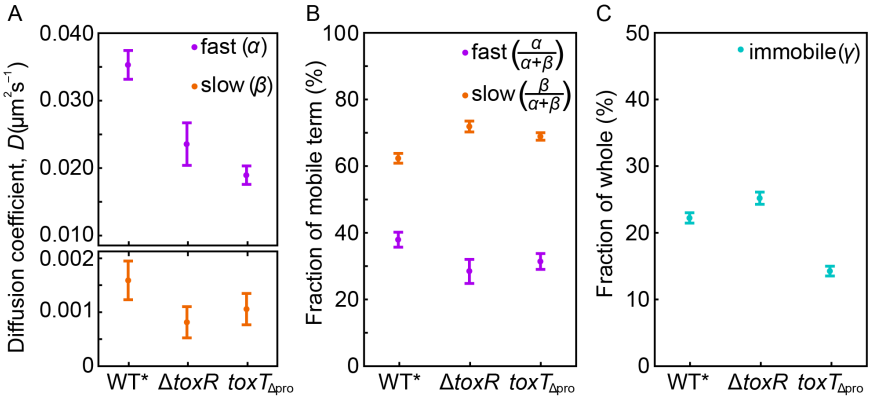

Fig. 6. Diffusion coefficients and fractional contributions from CPD analysis.
A. Diffusion coefficients for the 'fast' and 'slow' populations in all three strains, calculated from the MSD curves in Figs 2D and 5B and D. The bottom scale has been amplified to highlight differences among the values of the slow diffusion coefficient, D_β.
B. Contributions of the 'fast' and 'slow' populations to the mobile fraction for each strain.
C. Immobile fraction for each strain examined.
All error bars: ± 1 standard deviation.

Transient interactions with other membrane-associated proteins would also slow TcpP motion, but these encounters are expected to be more short-lived. As illustrated in Fig. S5A–D, respectively, TcpP interacting with DNA may move alone along the chromosome (Givaty and Levy, 2009); it may encounter nucleoid-associated proteins (NAPs; Nye *et al.*, 2000); it may bind non-specifically to some DNA region; or it may bind specifically to the *toxT* promoter (Goss *et al.*, 2010). Furthermore, TcpP might perform any of these motions while interacting with ToxR (Fig. S5E–H; Crawford *et al.*, 2003).

The CPDs of squared TcpP displacements indicate a significant immobile TcpP population in all three cell strains (Fig. 6C), yet this immobile fraction is significantly reduced in the promoter knockout strain ($toxT_{\Delta pro}$, γ = 14.1%) relative to the wild type-like strain (WT*, γ = 22.2%). In cells lacking $toxT_{pro}$, TcpP should spend more time engaged in non-specific sliding, hopping and scanning along DNA (green box in Fig. S5) because there is no specific binding target at which TcpP should become immobilized. Thus, the increase in the immobile fraction, which quantifies TcpP molecules that are essentially motionless between two consecutive imaging frames, is attributed to the binding of TcpP to the *toxT* promoter.

ToxR and $toxT_{pro}$ have similar impacts on 'fast' and 'slow' TcpP diffusion

Because a putative TcpP–ToxR–$toxT_{pro}$ complex would be much larger than TcpP alone, one might hypothesize that TcpP would move faster on its own than when interacting with ToxR, the *toxT* promoter, or both. Instead, the qualitative results from the histogram of displacements (Fig. 4) and the quantitative results from CPD analysis (Fig. 6; Table 3) both yield a surprising result: TcpP moves faster when it has the opportunity to interact with both ToxR and the *toxT* promoter than when either partner is missing (Fig. 6A; D_α and D_β are both maximum for WT*). Even more notably, deletions of either *toxR* or $toxT_{pro}$ have similar impacts on TcpP diffusion (Fig. 6A; D_α and D_β are nearly the same for Δ*toxR* and $toxT_{\Delta pro}$). Finally, comparing the contributions of the 'fast' and 'slow' populations (α and β respectively) to the total mobile fraction, when both ToxR and the *toxT* promoter are present (WT*), the 'fast' population makes up a larger component of the mobile term (Fig. 6B) relative to the knockout strains (Δ*toxR* and $toxT_{\Delta pro}$), which are similar.

The large impact of ToxR on the TcpP diffusion coefficients implies that ToxR molecules influence the motion of TcpP molecules for a significant amount of time, even when *toxT* transcription is not occurring. Previous work has shown that ToxR enhances the ability of TcpP to activate transcription of *toxT*: without ToxR, fewer modes of TcpP motion are possible (Fig. S5, red box), activation of *toxT* is greatly reduced, and only overexpression of TcpP can compensate (Higgins and DiRita, 1994; Häse and Mekalanos, 1998; Murley *et al.*, 1999; Krukonis *et al.*, 2000; Matson *et al.*, 2007). Taken together, these previous results, along with our new findings regarding TcpP motion, suggest that ToxR removes obstacles that prevent diffusing TcpP from reaching its $toxT_{pro}$ target. Furthermore, our finding that deleting $toxT_{pro}$ and deleting ToxR have similar impacts on the mobile ('fast' and 'slow') TcpP motion is surprising because there is only a single copy of the *toxT* promoter in each *V. cholerae* cell, while there are multiple copies of ToxR. Binding to the promoter must therefore enhance the interaction between ToxR and TcpP.

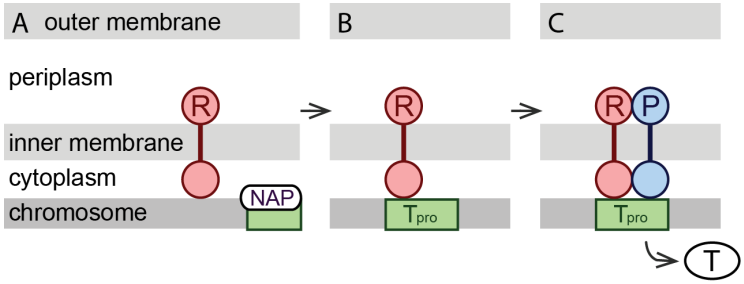

Fig. 7. Modified hand-holding mechanism for TcpP–ToxR–*toxT*$_{pro}$ interaction. ToxR scans along DNA, removing a nucleoid-associated protein (NAP) such as H-NS that occludes the *toxT* promoter (A). When ToxR subsequently binds to the *toxT* promoter (B), ToxR recruits TcpP, which activates ToxT transcription (C).

TcpP–ToxR–toxT$_{pro}$ interactions involve ToxR removing obstacles to TcpP diffusion

That ToxR increases TcpP mobility, and that this increased diffusion speed relies also on the *toxT* promoter must both figure significantly into the mechanism by which TcpP regulates ToxT expression. The increase in diffusion speed in the presence of additional interaction partners leads us to suggest involvement of nucleoid-associated proteins (NAPs), which bind large segments of bacterial DNA, compacting the chromosome and preventing excessive transcription (Dame *et al*., 2011; Wang *et al*., 2011). In *V. cholerae*, H-NS is a small, abundant NAP that binds the *toxT* promoter, as well as the *ctx* and *tcpA* promoters (Nye *et al*., 2000) and represses transcription at these sites. ToxT counteracts H-NS repression of *ctx* and *tcpA* (Nye *et al*., 2000; Yu and DiRita, 2002; Nye and Taylor, 2003), likely by displacing H-NS from the DNA (Stonehouse *et al*., 2011), and ToxR may do the same for *toxT* (Morgan *et al*., 2011). Indeed, in the absence of H-NS, neither TcpP nor ToxR are required for ToxT expression (Nye *et al*., 2000). If this is the case, ToxR may increase TcpP movement along DNA by removing the obstructing proteins; without ToxR, TcpP diffusion would be hindered.

Several models for the mechanism of ToxR–TcpP–*toxT*$_{pro}$ interaction have been proposed (Krukonis and DiRita, 2003b; Goss *et al*., 2010; 2013): these include the 'hand-holding' model, in which TcpP and ToxR interact directly while bound to the *toxT* promoter; the 'catch and release' model, in which ToxR releases TcpP upon DNA binding; the 'promoter alteration' model, in which the displacement of H-NS by ToxR bends or unwinds the promoter DNA, permitting TcpP recognition and binding; and the 'membrane recruitment' model, in which ToxR brings the *toxT* promoter closer to the inner membrane, facilitating TcpP binding at the promoter. All four of these models rely on ToxR displacing H-NS and recruiting TcpP to the *toxT* promoter. The hand-holding and catch and release models include direct interactions between ToxR and TcpP, while the ToxR–TcpP interaction in the promoter alteration and membrane recruitment models is indirect, and therefore these two models are inconsistent with our data, which show that a ToxR deletion reduces the diffusivity of TcpP.

Considering the impact of both ToxR and the *toxT* promoter on TcpP diffusion, the results of our CPD analysis are consistent with a mechanism in which ToxR enhances TcpP diffusion along DNA by removing occluding NAPs such as H-NS from the chromosome to facilitate TcpP diffusion, and ToxR also directly influences TcpP binding at the *toxT* promoter. To describe the TcpP–ToxR–*toxT*$_{pro}$ interaction, in Fig. 7, we therefore propose a variation of the hand-holding model. Here, when NAPs such as H-NS block the *toxT* promoter, ToxR molecules can remove these NAPs (Fig. 7A) to bind to the *toxT* promoter (Fig. 7B). In our model, ToxR then recruits TcpP to the exposed *toxT* promoter to activate *toxT* transcription (Fig. 7C). Thus, when ToxR is not present, the progress of TcpP is reduced, perhaps by the presence of H-NS, which makes it more difficult for *toxT* transcription to occur. TcpP overexpression might restore *toxT* activation by increasing the chances of any particular TcpP molecule locating the promoter (Higgins and DiRita, 1994; Häse and Mekalanos, 1998; Murley *et al*., 1999; Krukonis *et al*., 2000; Matson *et al*., 2007). Thus, the absence of *toxT*$_{pro}$ has a similar impact on TcpP diffusion as the absence of ToxR: ToxR is unable to bind, and thus cannot recruit TcpP. In this setting, TcpP may bind weakly and non-productively to DNA, and any movement along the DNA is disrupted by H-NS or other nucleoid-associated proteins.

Conclusions

The unusual membrane-bound transcription mechanism of the ToxR regulon remains key to understanding the virulence pathway in *V. cholerae*. Using super-resolution microscopy and single-molecule tracking with better than 40 nm resolution, we have examined the motions of TcpP, an essential ToxR regulon protein, in live cells. We found that TcpP labeled with PAmCherry retains its functionality and TcpP–PAmCherry localizes correctly to the inner membrane. We have compared TcpP displacement lengths and analyzed the cumulative probability distributions of these displacements for wild-type *V. cholerae* and for mutant strains that lack either *toxR* or the *toxT* promoter, and determined that TcpP mobility is enhanced

when both ToxR and $toxT_{pro}$ are present. Furthermore, a significant immobile TcpP population exists in all three strains, even when the *toxT* promoter has been removed and specific DNA binding therefore cannot occur. The evidence supports a mechanism in which ToxR recruits TcpP to $toxT_{pro}$; when ToxR is removed, TcpP is less likely to find the promoter, and when $toxT_{pro}$ is removed, TcpP is less likely to encounter ToxR.

Though rare, membrane-bound transcription activation is not restricted to *V. cholerae*; indeed similar mechanisms have been observed in several other organisms (Kolibachuk and Greenberg, 1993; Lin *et al*., 1993; Dell *et al*., 1994; Reich and Schoolnik, 1994; D'Elia and Salyers, 1996; Yang and Isberg, 1997; Welch and Bartlett, 1998; Blanc-Potard *et al*., 1999; Lassak *et al*., 2013). Investigating the specific role of TcpP in the *V. cholerae* virulence pathway will then also shed light on the mechanisms and dynamics of membrane-bound transcription regulation in general. Future experiments labeling ToxR or the DNA near the *toxT* promoter will enable dual-color imaging of this transcription activation mechanism, lead to greater understanding of the role of NAPs in the regulation of transcription, and offer additional insight into molecular-scale interactions. Furthermore, the mechanism by which the membrane localized complex recruits RNA polymerase remains a significant gap in our understanding of how such activators stimulate transcription, and future efforts to uncover this process will complement our current research directions.

Experimental procedures

Bacterial strains and plasmid construction

The *V. cholerae* classical strain O395 was used throughout this study. The *Escherichia coli* strain JM101 was used for cloning. The *tcpP–PAmCherry* chimeric gene was constructed as follows: *tcpP* (lacking the stop codon) was amplified from O395 chromosomal DNA using Expand Hi-Fidelity polymerase. Photoactivatable (PA)-mCherry was amplified from pPAmCherry N1 (Clontech; Subach *et al*., 2009). A secondary SOEing PCR using the *tcpP* and PAmCherry PCR products as template DNA was used to generate the fusion gene. The resulting PCR product was digested with EcoRI and XbaI and ligated into similarly digested pBAD18-Kan (Guzman *et al*., 1995). The resulting plasmid was confirmed by sequencing and transformed into *V. cholerae* strains by electroporation. The TcpP–PAmCherry fusion protein was expressed in the following previously described strains for visualization and localization studies: O395 Δ*tcpP* (RY1; Yu and DiRita, 1999), O395 Δ*tcpP* Δ*toxR* (EK459; Krukonis *et al*., 2000), and O395 Δ*tcpP* $toxT_{\Delta pro}$ (EK1647; Goss *et al*., 2010; Table 1).

Protein electrophoresis and immunodetection

Overnight cultures of *V. cholerae* were subcultured 1:100 in pH 6.5 LB and grown for 4 h at 30°C. Arabinose was added to the culture medium at the time of subculture for strains containing pBAD18-Kan. One milliliter of mid-log culture was pelleted by centrifugation and resuspended in 1× sample buffer. Proteins were separated by SDS-polyacrylamide gel electrophoresis (SDS-PAGE) using 15% (wt/vol) polyacrylamide gels. Samples were boiled for 5 min before loading on the gels and loading volumes were adjusted to normalize for culture OD_{600}. Proteins were then transferred to nitrocellulose membranes and probed with rabbit anti-TcpP antibodies (generated by Rockland) or rabbit anti-TcpA antibody (generously supplied by Dr. Ronald Taylor). Blots were probed with goat anti-rabbit AP-conjugated secondary antibody (Zymed) followed by visualization using NBT-BCIP (nitroblue tetrazolium and 5-bromo-4-chloro-3-indolylphosphate; Roche).

qRT-PCR analysis

Triplicate cultures of O395, O395 Δ*tcpP*, and WT* were grown and induced as above. Equivalent numbers of cells from each sample were harvested and RNA was extracted using TRIzol reagent (Life Technologies). RNA samples for qRT-PCR were DNase treated, run on an agarose gel to check quality, and quantified by measuring the OD_{260}. Two and half micrograms of each sample were treated with Moloney murine leukemia virus (M-MLV) reverse transcriptase (Invitrogen) according to the manufacturer's specifications. For detection of transcripts, primers amplifying a 200 bp region in the center of the mRNA were used with SYBR Green Master Mix (Stratagene) on a Stratagene MX3000P thermocycler. Primers were designed using the OligoPerfect tool (Invitrogen). Each test was performed in triplicate at least three times, and fold change in expression was calculated using the ΔΔCT method with *recA* transcript levels as the reference.

Cell growth and sample preparation for microscopy

Bacterial cultures were grown in LB medium at 37°C with shaking (180 r.p.m.), then transferred to M9 minimal medium with 0.4% glycerol and an amino acid supplement (asparagine, arginine, glutamic acid and serine, 25 mM final concentration) and grown to turbidity at 30°C. Kanamycin (50 μg ml^{-1} final concentration) was used to select for the plasmid. Arabinose (0.1% final concentration) was added to the cultures to induce expression of the fusion protein and the cultures were incubated for an additional 4 h. A 1 ml aliquot of culture was centrifuged for 30 s at 30 000 *g* to pellet the cells. The pellet was washed in 1 ml warm M9, and centrifuged a second time. The supernatant was then removed, and the cell pellet was resuspended in a minimum of residual liquid (< 100 μl). A 2.0 μl droplet of concentrated cells was then placed onto an agarose pad (2% agarose dissolved in M9, spread on a microscope slide) and covered with a coverslip.

Super-resolution microscopy

Samples were imaged at room temperature using wide-field epifluorescence microscopy on an Olympus IX71 inverted microscope with a 100×, 1.40 NA oil immersion objective (Zeiss Immersol 518F immersion oil), a Semprex micrometer stage, a PIFOC piezo element, and appropriate excitation,

emission, and dichroic filters (Semrock LL01-407, Semrock LL01-561, Semrock BLP01-561, Semrock Di01-R561). A Photometrics Evolve EMCCD camera with > 90% quantum efficiency was used to capture the images at 20 frames per second. Each pixel of the detector corresponds to a 49×49 nm area of the sample. Fluorescence of PAmCherry in the cells was activated using a 405 nm laser (Coherent Cube 405-100), co-aligned with the 561 nm fluorescence excitation laser (Coherent Sapphire 560-50). The lasers were both operated at low power densities (0.006–0.2 $\mu W\ \mu m^{-2}$ and 0.2–0.3 $\mu W\ \mu m^{-2}$ respectively). The excitation and activation pathways were coupled by a dichroic mirror (Semrock Di01-R405), and both laser beams were circularly polarized (Tower Optical AO15Z 1/4 556, Tower Optical AO15Z 1/4 408). To prevent higher-order excitation during photoactivation, a pair of Uniblitz shutters controlled the laser beams such that samples were exposed to only one laser at a time. During imaging, the cells were given a 70 ms dose of 405 nm light every 90 s. Acquisitions lasted 5–7 min each.

Single fluorophores were localized using custom MATLAB code (Biteen *et al*., 2008) that detects diffraction-limited local intensity maxima above a specified background threshold and fits their point-spread functions (PSFs) to symmetric two-dimensional Gaussian functions (Thompson *et al*., 2002). The output of this code includes positions in *x* and *y*, and the 95% confidence intervals for these positions, which were used to estimate the localization error. The super-resolution reconstruction images in Figs 2A and 3A and C show single-molecule localizations blurred to these confidence intervals.

Single-molecule trajectories were determined using custom MATLAB code employing a nearest-neighbor algorithm: molecules localized in consecutive frames within six pixels (294 nm) of each other were considered members of the same track. Only trajectories with at least 10 frames were used for further analysis to obtain the best estimate of the diffusion coefficient (Michalet, 2011).

Acknowledgements

This work was supported in part by a Burroughs Wellcome Fund Career Award at the Scientific Interface to JSB and by National Institutes of Health (NIAID) Grant R21-AI099497-02 to VJD and JSB. We thank Aaron Konopko for assistance with the qRT-PCR experiment, and Chanrith Siv, Hannah Tuson and Yi Liao for helpful comments.

References

Bakshi, S., Siryaporn, A., Goulian, M., and Weisshaar, J.C. (2012) Superresolution imaging of ribosomes and RNA polymerase in live *Escherichia coli* cells. *Mol Microbiol* **85:** 21–38.

Beck, N.A., Krukonis, E.S., and DiRita, V.J. (2004) TcpH influences virulence gene expression in *Vibrio cholerae* by inhibiting degradation of the transcription activator TcpP. *J Bacteriol* **186:** 8309–8316.

Berk, V., Fong, J.C.N., Dempsey, G.T., Develioglu, O.N., Zhuang, X., Liphardt, J., *et al*. (2012) Molecular architecture and assembly principles of *Vibrio cholerae* biofilms. *Science* **337:** 236–239.

Betzig, E., Patterson, G.H., Sougrat, R., Lindwasser, O.W., Olenych, S., Bonifacino, J.S., *et al*. (2006) Imaging intracellular fluorescent proteins at nanometer resolution. *Science* **313:** 1642–1645.

Biteen, J.S., Thompson, M.A., Tselentis, N.K., Bowman, G.R., Shapiro, L., and Moerner, W.E. (2008) Super-resolution imaging in live *Caulobacter crescentus* cells using photoswitchable EYFP. *Nat Methods* **5:** 947–949.

Blanc-Potard, A., Solomon, F., Kayser, J., and Groisman, E.A. (1999) The SPI-3 pathogenicity island of *Salmonella enterica*. *J Bacteriol* **181:** 998–1004.

Cravioto, A., Lanata, C.F., Lantagne, D.S., and Nair, G.B. (2011). Final report of the independent panel of experts on the cholera outbreak in Haiti [WWW document]. URL http://www.un.org/News/dh/infocus/haiti/UN-cholera-report-final.pdf

Crawford, J.A., Krukonis, E.S., and DiRita, V.J. (2003) Membrane localization of the ToxR winged-helix domain is required for TcpP-mediated virulence gene activation in *Vibrio cholerae*. *Mol Microbiol* **47:** 1459–1473.

Dame, R.T., Kalmykowa, O.J., and Grainger, D.C. (2011) Chromosomal macrodomains and associated proteins: implications for DNA organization and replication in Gram negative bacteria. *PLoS Genet* **7:** e1002123.

Dell, C.L., Neely, M.N., and Olson, E.R. (1994) Altered pH lysine signalling mutants of *cadC* a gene encoding a membrane-bound transcriptional activator of the *Escherichia coli cadBA* operon. *Mol Microbiol* **14:** 7–16.

D'Elia, J.N., and Salyers, A.A. (1996) Effect of regulatory protein levels on utilization of starch by *Bacteroides thetaiotaomicron*. *J Bacteriol* **178:** 7180–7186.

Givaty, O., and Levy, Y. (2009) Protein sliding along DNA: dynamics and structural characterization. *J Mol Biol* **385:** 1087–1097.

Goss, T.J., Seaborn, C.P., Gray, M.D., and Krukonis, E.S. (2010) Identification of the TcpP-binding site in the *toxT* promoter of *Vibrio cholerae* and the role of ToxR in TcpP-mediated activation. *Infect Immun* **78:** 4122–4133.

Goss, T.J., Morgan, S.J., French, E.L., and Krukonis, E.S. (2013) ToxR recognizes a direct repeat element in the *toxT*, *ompU*, *ompT*, and *ctxA* promoters of *Vibrio cholerae* to regulate transcription. *Infect Immun* **81:** 884–895.

Griffin, B.A., Adams, S.R., and Tsien, R.Y. (1998) Specific covalent labeling of recombinant protein molecules inside live cells. *Science* **281:** 269–272.

Guzman, L.M., Belin, D., Carson, M.J., and Beckwith, J. (1995) Tight regulation, modulation, and high-level expression by vectors containing the arabinose PBAD promoter. *J Bacteriol* **177:** 4121–4130.

Haas, B.L., Matson, J.S., DiRita, V.J., and Biteen, J.S. (2014) Live-cell super-resolution fluorescence microscopy: obstacles and achievements in experimental optimization for microbiology. *Molecules* **19:** 12116–12149.

Häse, C.C., and Mekalanos, J.J. (1998) TcpP protein is a positive regulator of virulence gene expression in *Vibrio cholerae*. *Proc Natl Acad Sci USA* **95:** 730–734.

Hess, S.T., Girirajan, T.P.K., and Mason, M.D. (2006) Ultra-high resolution imaging by Fluorescence Photoactivation Localization Microscopy. *Biophys J* **91:** 4258–4272.

Higgins, D.E., and DiRita, V.J. (1994) Transcriptional control of *toxT* a regulatory gene in the ToxR regulon of *Vibrio cholerae*. *Mol Microbiol* **14:** 17–29.

Jaqaman, K., Loerke, D., Mettlen, M., Kuwata, H., Grinstein, S., Schmid, S.L., and Danuser, G. (2008) Robust single-particle tracking in live-cell time-lapse sequences. *Nat Methods* **5:** 695–702.

Kim, S.Y., Gitai, Z., Kinkhabwala, A., Shapiro, L., and Moerner, W.E. (2006) Single molecules of the bacterial actin MreB undergo directed treadmilling motion in *Caulobacter crescentus*. *Proc Natl Acad Sci USA* **103:** 10929–10934.

Kolibachuk, D., and Greenberg, E.P. (1993) The *Vibrio fischeri* luminescence gene activator LuxR is a membrane-associated protein. *J Bacteriol* **175:** 7307–7312.

Krukonis, E.S., and DiRita, V.J. (2003a) From motility to virulence: sensing and responding to environmental signals in *Vibrio cholerae*. *Curr Opin Microbiol* **6:** 186–190.

Krukonis, E.S., and DiRita, V.J. (2003b) DNA binding and ToxR responsiveness by the wing domain of TcpP, an activator of virulence gene expression in *Vibrio cholerae*. *Mol Cell* **12:** 157–165.

Krukonis, E.S., Yu, R.R., and DiRita, V.J. (2000) The *Vibrio cholerae* ToxR/TcpP/ToxT virulence cascade: distinct roles for two membrane-localized transcriptional activators on a single promoter. *Mol Microbiol* **38:** 67–84.

Lassak, K., Peeters, E., Wróbel, S., and Albers, S. (2013) The one-component system ArnR: a membrane-bound activator of the crenarchaeal archaellum. *Mol Microbiol* **88:** 125–139.

Lin, Z., Kumagai, K., Baba, K., Mekalanos, J.J., and Nishibuchi, M. (1993) *Vibrio parahaemolyticus* has a homolog of the *Vibrio cholerae toxRS* operon that mediates environmentally induced regulation of the thermostable direct hemolysin gene. *J Bacteriol* **175:** 3844–3855.

Lommerse, P.H.M., Blab, G.A., Cognet, L., Harms, G.S., Snaar-Jagalska, B., Spaink, H.P., and Schmidt, T. (2004) Single-molecule imaging of the H-Ras membrane-anchor reveals domains in the cytoplasmic leaflet of the cell membrane. *Biophys J* **86:** 609–616.

Matson, J.S., Withey, J.H., and DiRita, V.J. (2007) Regulatory networks controlling *Vibrio cholerae* virulence gene expression. *Infect Immun* **75:** 5542–5549.

Mekalanos, J.J. (2010) The evolution of *Vibrio cholerae* as a pathogen. In *Epidemiological and Molecular Aspects on Cholera*. Ramamurthy, T., and Bhattacharya, S.K. (eds). New York, NY: Humana Press, pp. 97–114.

Michalet, X. (2011) Mean square displacement analysis of single-particle trajectories with localization error: Brownian motion in an isotropic medium. *Phys Rev E Stat Nonlin Soft Matter Phys* **82:** 041914.

Morgan, S.J., Felek, S., Gadwal, S., Koropatkin, N.M., Perry, J.W., Bryson, A.B., and Krukonis, E.S. (2011) The two faces of ToxR: activator of *ompU* co-regulator of *toxT* in *Vibrio cholerae*. *Mol Microbiol* **81:** 113–128.

Murley, Y.M., Carroll, P.A., Skorupski, K., Taylor, R.K., and Calderwood, S.B. (1999) Differential transcription of the *tcpPH* operon confers biotype-specific control of the *Vibrio cholerae* ToxR virulence regulon. *Infect Immun* **67:** 5117–5123.

Nye, M.B., and Taylor, R.K. (2003) *Vibrio cholerae* H-NS domain structure and function with respect to transcriptional repression of ToxR regulon genes reveals differences among H-NS family members. *Mol Microbiol* **50:** 427–444.

Nye, M.B., Pfau, J.D., Skorupski, K., and Taylor, R.K. (2000) *Vibrio cholerae* H-NS silences virulence gene expression at multiple steps in the ToxR regulatory cascade. *J Bacteriol* **182:** 4295–4303.

Qian, H., Sheetz, M.P., and Elson, E.L. (1991) Single particle tracking. Analysis of diffusion and flow in two-dimensional systems. *Biophys J* **60:** 910–921.

Reich, K.A., and Schoolnik, G.K. (1994) The light organ symbiont *Vibrio fischeri* possesses a homolog of the *Vibrio cholerae* transmembrane transcriptional activator ToxR. *J Bacteriol* **176:** 3085–3088.

Rust, M.J., Bates, M., and Zhuang, X. (2006) Sub-diffraction-limit imaging by Stochastic Optical Reconstruction Microscopy (STORM). *Nat Methods* **3:** 793–795.

Schütz, G.J., Schindler, H., and Schmidt, T. (1997) Single-molecule microscopy on model membranes reveals anomalous diffusion. *Biophys J* **73:** 1073–1080.

Sochacki, K.A., Shkel, I.A., Record, M.T., and Weisshaar, J.C. (2011) Protein diffusion in the periplasm of *E. coli* under osmotic stress. *Biophys J* **100:** 22–31.

Sonnleitner, A., Schütz, G.J., and Schmidt, T. (1999) Free Brownian motion of individual lipid molecules in biomembranes. *Biophys J* **77:** 2638–2642.

Stonehouse, E.A., Hulbert, R.R., Nye, M.B., Skorupski, K., and Taylor, R.K. (2011) H-NS binding and repression of the *ctx* promoter in *Vibrio cholerae*. *J Bacteriol* **193:** 979–988.

Subach, F.V., Patterson, G.H., Manley, S., Gillette, J.M., Lippincott-Schwartz, J., and Verkhusha, V.V. (2009) Photoactivatable mCherry for high-resolution two-color fluorescence microscopy. *Nat Methods* **6:** 153–159.

Thompson, R.E., Larson, D.R., and Webb, W.W. (2002) Precise nanometer localization analysis for individual fluorescent probes. *Biophys J* **82:** 2775–2783.

Wang, W., Li, G., Chen, C., Xie, X.S., and Zhuang, X. (2011) Chromosome organization by a nucleoid-associated protein in live bacteria. *Science* **333:** 1445–1449.

Welch, T.J., and Bartlett, D.H. (1998) Identification of a regulatory protein required for pressure-responsive gene expression in the deep-sea bacterium *Photobacterium* species strain SS9. *Mol Microbiol* **27:** 977–985.

van den Wildenberg, S.M.J.L., Bollen, Y.J.M., and Peterman, E.J.G. (2011) How to quantify protein diffusion in the bacterial membrane. *Biopolymers* **95:** 312–321.

Xie, X.S., Choi, P.J., Li, G.W., Lee, N.K., and Lia, G. (2008) Single-molecule approach to molecular biology in living bacterial cells. *Annu Rev Biophys* **37:** 417–444.

Yang, Y., and Isberg, R.R. (1997) Transcriptional regulation of the *Yersinia pseudotuberculosis* pH 6 antigen adhesin by two envelope-associated components. *Mol Microbiol* **24:** 499–510.

Yu, R.R., and DiRita, V.J. (1999) Analysis of an autoregulatory loop controlling ToxT cholera toxin, and toxin-coregulated pilus production in *Vibrio cholerae*. *J Bacteriol* **181:** 2584–2592.

Yu, R.R., and DiRita, V.J. (2002) Regulation of gene expression in *Vibrio cholerae* by ToxT involves both antirepression and RNA polymerase stimulation. *Mol Microbiol* **43:** 119–134.

Supporting information

Additional supporting information may be found in the online version of this article at the publisher's web-site.